First sky tests of adaptive optics predictive control*

C. Dessenne, P.-Y. Madec, D. Rabaud, B. Fleury and G. Rousset

Office National d'Études et de Recherches Aérospatiales (ONERA)
Département d'Optique Théorique et Appliquée
BP 72, F-92322 Châtillon cedex, France
* Comments to: madec@onera.fr

Abstract – One of the main limitations to adaptive optics (AO) correction efficiency is the time lag in the loop due to wave-front time averaging, digital-to-analog conversion of deformable mirror control voltages and read-out of the wave-front sensor (WFS) detector. It has been shown that Shack-Hartmann WFS measurements are predictible. More recently, we studied closed-loop prediction for AO control and synthesized a linear modal predictor. In this paper, the theory of modal predictive control in AO is reminded. Numerical and laboratory results are presented, where the ONERA AO system including a modal predictive control is used with a turbulence simulation cell. Finally, first results obtained on sky at the focus of the 1.52 m telescope at Observatoire de Haute-Provence are given and discussed. They show the significant gain which can be brought by using modal predictive control instead of conventional control algorithms.

1 Introduction

The performance of the servo loop of an adaptive optics (AO) system is limited by measurement noise and time delay in terms of residual optical phase variance. The optimization of the AO control against both limitations is a key issue to enhance the quality of corrected images. Optimized modal control [1, 2] has been developed in which the gain of an integral controller is optimized mode by mode, depending on the level of noise and turbulence. This is today the most effective controller used on operational AO systems [3]. However, it does not reduce the effects of time delay. It has been demonstrated that turbulence measured by a Shack-Hartmann wave-front sensor (SH WFS) is predictible [4, 5] and that open-loop predictors [6, 7, 8, 9] can provide significant improvement. Three theoretical approaches to the closed-loop problem have been proposed: a zonal one [10], a modal state space one [11] and a modal one [12, 13] which is based on a transfer-function approach.

In this paper, the theory of modal predictive control [12, 13] in AO and numerical results previously published [12] are briefly reminded. Experimental results obtained with the ONERA AO system are described. We report experiments carried out in laboratory with a turbulence simulation cell and at the focus of the 1.52 m telescope at Observatoire de Haute-Provence (OHP, France) observing sky objects.

2 The theory of modal and linear predictive control [12]

2.1 Description of the servo loop

2.1.1 Notations

In the following, $\mathcal{X}(s)$, $\tilde{x}(j\omega)$ and $\mathcal{X}(z)$ are respectively the Laplace, Fourier and $\mathcal{Z}$ transforms of a variable x where $j^2 = -1$ and ω is the pulsation. ω is normalized to the sampling frequency $f_s = 1/T$, i.e. $\omega = 2\pi fT$, where f is the frequency and T is the sampling period of the WFS, equal to the sampling period of the servo loop. $x(t)$ and $x(k)$ are x at time t and kT. When we write $\tilde{x} = \mathcal{H}\tilde{y}$, x and y being any variable and $\mathcal{H}$ a transfer function, we mean $\tilde{x}(j\omega) = \mathcal{H}(s{=}j\omega)\tilde{y}(j\omega)$ if $\mathcal{H}$ is a Laplace transfer function and $\tilde{x}(j\omega) = \mathcal{H}(z{=}\mathrm{e}^{j\omega})\tilde{y}(j\omega)$ if $\mathcal{H}$ is a sampled transfer function.

2.1.2 Hypotheses

The performance of the AO servo loop is analyzed in terms of N independent monovariable servo loops, where N is the number of deformable mirror (DM) actuators. Each monovariable servo loop describes the correction of a mode $M_i(\vec{r})$ of an orthogonal basis $(M_i(\vec{r}))_{1\leq i\leq N}$. The N modes being orthogonal, the total compensated residual variance is the sum of each residual mode variance. It is equivalent to minimize the total residual variance, which is the optimization criterion used in this paper, and to optimize the residual variance of N monovariable servo loops. The theoretical developments presented in this paper concern the optimization of one monovariable servo loop.

We consider the servo loop is linear and assume the measurement noise is white and decorrelated from the turbulent input.

2.1.3 Transfer functions

The block diagram of the system is shown in Fig. 1. It is divided into six physical blocks: the WFS which measures the phase distortions averaged during an exposure time T, the wave-front computer which reads the signal from the WFS detector and reconstructs the control mode with a computing time τ, the predictor of transfer function $\mathcal{P}$ which computes the voltage to be applied to the DM and acts as a temporal compensator, the digital-to-analog converters, the high-voltage amplifiers which transform the low voltage output of the converters into high voltages to control the DM actuators and the DM which corrects the mode. ε is the residual control mode, n is the measurement noise and ε_{meas} is the control mode measured by the SH WFS.

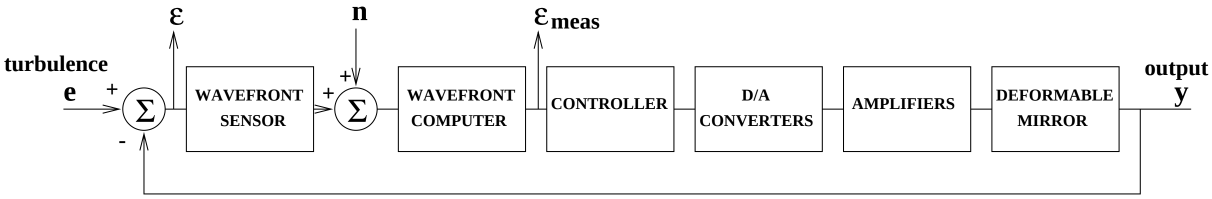

FIG. 1: *Block diagram of an AO system.*

The open-loop transfer function $\mathcal{H}$ is the product of the transfer functions of all the components. It is equal to [14]:

$$\mathcal{H}(s) = \left[\frac{1-\mathrm{e}^{-\mathrm{T}s}}{Ts}\right]^2 \mathrm{e}^{-\tau s}\mathcal{P}(z{=}\mathrm{e}^{+Ts}). \tag{1}$$

The loop exhibits an overall time delay of $\tau + T$ including averaging of the turbulent mode by the SH WFS and digital-to-analog conversion. In this paper, we will consider $\tau \simeq T$, which corresponds to the general case of a SH WFS. For $\tau = T$, $\mathcal{H}(s)$ can be rewritten as the following sampled transfer function:

$$\mathcal{H}(z) = z^{-2}\mathcal{P}(z). \tag{2}$$

In Fig. 2, a $\mathcal{Z}$ block diagram for the servo loop is presented when $\tau = T$. Such system has no dynamical characteristic and is described by a time delay of two sampling frames.

In the following, the open loop is referred to as measurements of the turbulent wave front (i.e. the outputs of the wave-front computer) when the DM is not controlled. If e_{meas} and ε_{meas} are the open-loop and closed-loop measurements, we show that:

$$\tilde{\varepsilon}_{meas} = \frac{\tilde{e}_{meas}}{1+\mathcal{H}}. \tag{3}$$

$1/(1+\mathcal{H})$ is called the error transfer function: it characterizes the attenuation of the turbulent mode by the loop.

2.2 Determination of $\mathcal{P}$

$\mathcal{P}$ is determined by minimizing the residual mean square error (MSE) $\langle\varepsilon^2\rangle$ of the control mode. For a white noise decorrelated from the signal, we show that it is equivalent to minimize $\langle\varepsilon^2\rangle$ and $\langle\varepsilon^2_{meas}\rangle$ [12].

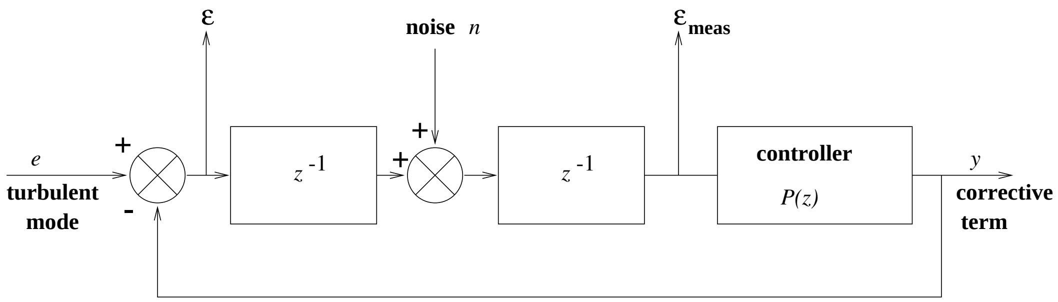

FIG. 2: *Sampled block diagram of an AO system for* $\tau = T$.

Ideally, the residual MSE $\langle \varepsilon^2 \rangle$ is equal to 0. ε_{meas} is then a white noise of variance $\langle n^2 \rangle$. We show that this leads to [12]:

$$\forall \omega,\ \left|\left|\mathcal{P}_{ideal}(z{=}\mathrm{e}^{+j\omega})\right|\right|^2 = \frac{||\tilde{e}(j\omega)||^2}{\langle n^2 \rangle / 2\pi} \tag{4}$$

This ideal predictor perfectly compensates for the time delay in the servo loop. It is defined by the spectral signal-to-noise ratio of the turbulent control mode. However, it can be shown that the ideal predictor leads to an unstable AO system. We therefore define an optimal predictor which best fits the spectral signal-to-noise ratio. Let us note that the temporal information about turbulence, like wind speed, is contained in the spectral signal-to-noise ratio through $||\tilde{e}(j\omega)||^2$.

In practice, $\mathcal{P}$ is defined by a recursive equation:

$$y(k) = -\sum_{i=1}^{p-1} b_i \varepsilon_{meas}(k-i) \sum_{i=0}^{q-1} b_i y(k-i) \tag{5}$$

where y is the output of the predictor, ε_{meas} its input, k the time step, and p and q the orders of the predictor. The parameters a_i and b_i are derived by minimizing $\langle \varepsilon^2_{meas} \rangle$ under AO system stability constraint. A classical recursive least square algorithm [15] is modified to take account of the closed-loop recursivity. The input of this algorithm is e_{meas}, the open-loop measurements of each control mode.

3 Performance of the predictor: numerical simulations [12]

A Kolmogorov turbulent phase is simulated [16] with 861 turbulent Zernike modes corresponding to a Hufnagel vertical C_n^2 profile and a AMOS [17] (Air Force Maui Optical Station) average vertical wind speed profile. The wave front is measured by a 9×9 sub-aperture SH WFS in a pupil of diameter $D = 8$ m with no central obscuration. From the slope measurements, 44 Zernike modes (piston is excluded) are reconstructed. The 44 Zernike modes are the control modes. We consider the DM is able to produce them for the correction. The white noise in the measurement is propagated on them through the reconstruction matrix. The signal-to-noise ratio (SNR) is expressed as the ratio of the open-loop SH measurement turbulence variance to the measurement noise variance. The general conditions are $D/r_0 = 10$ and $V/D = 2$ Hz where r_0 is the Fried diameter and V is the mean wind speed along the optical path. The outer scale of the turbulence is supposed infinite. The data are stationary and centered. Two sampling frequencies are tested: $f_s = 50$ Hz and $f_s = 100$ Hz.

The performance of the predictor is analyzed in terms of Strehl ratio (S_r) computed from the simulation of corrected images. The predictor is compared to an integral controller, defined by the recursive equation $y(k) = y(k-1) + K\varepsilon_{meas}(k)$ where K is the gain of the controller, since optimized integral controllers are currently the best implemented controllers on operational adaptive optics systems. Both controllers are optimized mode by mode. Fig. 3 presents S_r versus SNR for a 6 parameter predictor and the two different sampling frequencies f_s. It shows that there is more to gain with the predictor when the SNR is high. Since the predictor parameters minimize the residual MSE, the predictor filters noise at low SNRs, while it reduces the temporal error due to time delay at high SNRs, which means it predicts. The predictor performs much better than the integral controller for low f_s, or equivalently high V at a given f_s. Indeed, f_s is influential through the ratio $(V/D)/f_s$ which is proportional to the ratio of the power spectral density cut-off frequency of each mode [18] to the sampling frequency. The interest of the predictor is more obvious when the phase distortion is changing rapidly than when it is slow, compared to the AO system bandwidth.

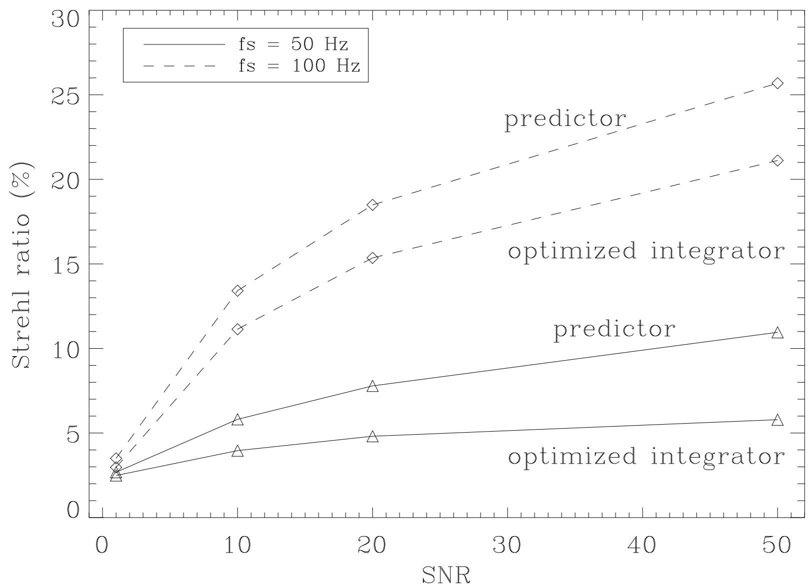

FIG. 3: *Numerical simulations: Strehl ratio versus SNR for two different sampling frequencies. Comparison between the predictor and the integral controller. Conditions: $\tau = T$, V/D = 2 Hz, D/r_0 = 10, 6 parameter predictor.*

4 Performance of the predictor: laboratory experiments

The model of the AO system and the numerical results are now validated by experiments in laboratory with a real AO system.

4.1 Description

The wave-front disturbances are generated by a turbulence simulation cell with the following turbulence parameters: $D/L_0 \approx 0.6$, $D/r_0 \approx 10$ at 0.65 μm and $\overline{V}/D \approx 8$ Hz. These conditions are stationary. The ONERA AO system is equipped with a 9 by 9 sub-aperture SH WFS whose detector is an intensified CCD camera, an 88 actuator DM [1] and a fast tip-tilt mirror [2] (TTM). A 6 parameter predictor is implemented on the C40 based real time computer [3]. Different sampling frequencies f_s and different SNRs are tested. Therefore, we set different values for the ratio $(V/D)/f_s$ by changing f_s rather than V. Four different f_s are tested. SNR is changed by adding a density which can dim the intensity of the light reaching the SH WFS and by varying the intensity of the light source.

For each controller (integrator or predictor) and for a given couple (SNR, f_s), optimization of the controller parameters is followed by operation in closed loop using the optimized parameters. This process is repeated 10 times for each couple. The corrected images are recorded by a 512 by 512 pixel CCD camera at 0.65 μm. S_r is computed

1. CILAS
2. Physik Instrumente
3. SHAKTI

and averaged to give an estimation of S_r. Closed-loop WFS measurements are recorded to compute residual MSE and estimate the error transfer functions $1/(1+\mathcal{H})$.

Figure 4 presents the gain of the error transfer function for one TTM axis. The dotted line shows the transfer function which is expected from AO system modeling, including the parameters of the predictor. The full line is an estimation of the transfer function of the real system [13]. This estimation is based on Eq. (3). There is a very good agreement between our model and what is actually measured. This proves that our model of the system is correct.

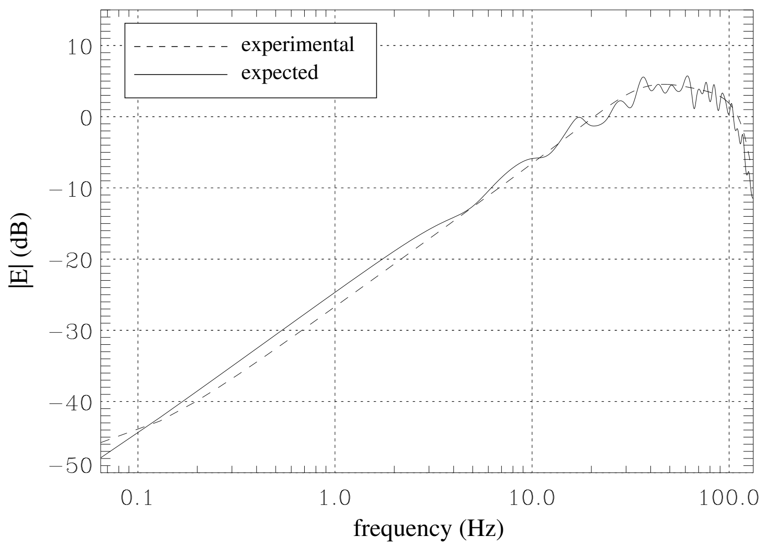

FIG. 4: *Laboratory experiments: experimental (full line) and expected (dashed line) gains of the error transfer function for a tip-tilt mode. f_s = 264 Hz, SNR = 14.5.*

4.2 Performance of the predictor

Measured Strehl ratios for different SNRs and sampling frequencies are presented in Fig. 5. The measured average number of photons detected by sampling period and per sub-pupil after thresholding is indicated. The dotted and full line represent the optimized integrator and the predictor respectively. The trends are very similar to what was presented in previous section for numerical simulations (Fig. 3), although conditions in terms of number of control modes and outer scale are different. The predictor is more interesting for high SNR and low f_s, as expected. However, its efficiency is always better than that of an integrator. This is due to the residual MSE minimization scheme.

The aim of modal control is to control each of the modes with different controller parameters. From closed-loop WFS SH measurements, the measured residual MSE $\langle\varepsilon_i^2\rangle$ of control mode i can be estimated. A modal gain $1-\langle\varepsilon_{i,pred}^2\rangle/\langle\varepsilon_{i,integ}^2\rangle$ is defined. Indices *pred* and *integ* stand for the predictive and integral controller respectively. The higher the gain, the more the system benefits from the control of mode i with the predictor.

Fig. 6 presents this modal gain as a function of control mode number. The 10 first control modes have been filtered out from the control matrix and do not appear on this graph. The last two modes correspond to the TTM. A relative gain of about 20% in terms of residual MSE is measured at $f_s = 533$ Hz and SNR $= 9.1$. This gain is of course dependent on f_s and SNR. The full diamonds show the gain which is measured on the real system operating in closed loop. The expected gain, presented in empty diamonds, is computed from open-loop measurements using a model of the system. The agreement between the expected and the measured gain is excellent, which once again confirms the model used in the theoretical developments.

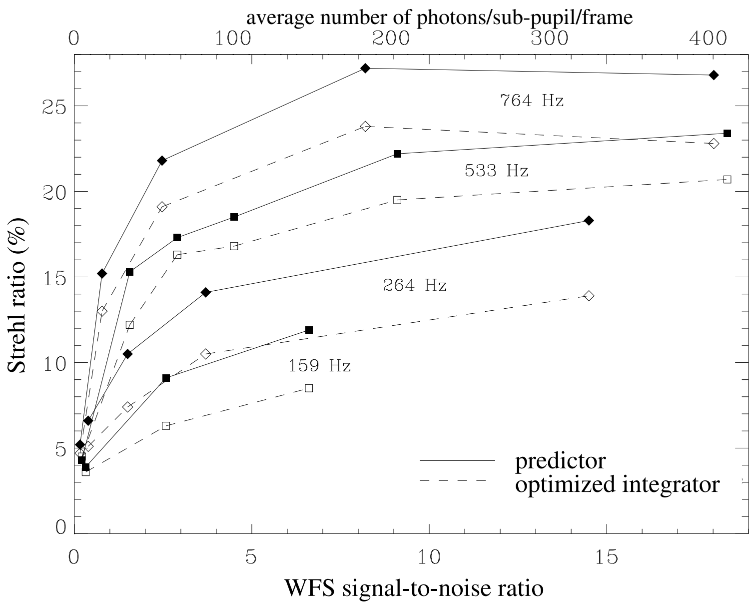

FIG. 5: *Laboratory experiments: Strehl ratio measured on corrected images as a function of the signal-to-noise ratio and the sampling frequency for both controllers.* $D/r_0 = 10$, $D/L_0 = 0.65$ *and* $V/D = 8$ *Hz.*

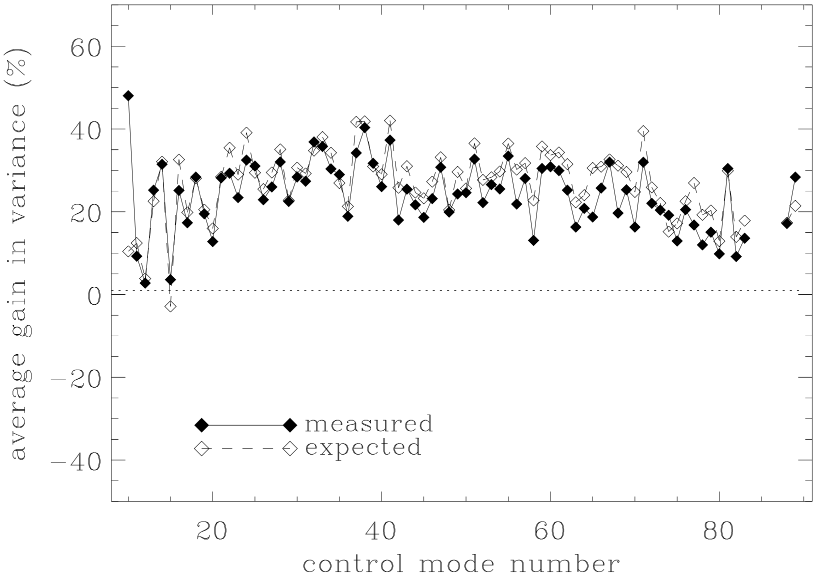

FIG. 6: *Laboratory experiments: normalized average expected and measured gain in residual mean square error as a function of the control mode number.* $f_s = 533$ *Hz, SNR = 9.1.*

5 Performance of the predictor: experiments at Observatoire de Haute-Provence

The final step in the experimental validation of the predictor efficiency is to observe sky objects in real experimental conditions. This was done by using the ONERA AO system at a wavelength of 0.65 μm at the focus of the 1.52 m telescope at Observatoire de Haute-Provence (OHP, France).

5.1 Validation of modal prediction in real conditions

We report a first experiment which was carried out during the night from 09/30/97 to 10/01/97 observing two unresolved stars. β Andromedae, of magnitude 2.06, was observed between 19h43 UT and 22h04 UT. ξ Cygni, of magnitude 3.72, was observed between 22h26 UT and 00h33 UT. A density was included in the AO system just before the SH WFS to dim the intensity of the light. The equivalent magnitudes from the SH WFS point of view were respectively 6.06 and 6.72. The sampling frequency was $f_s = 264$ Hz for β Andromedae and 159 Hz for ξ Cygni.

For both objects, series of 20 sequences of open-loop followed by closed-loop SH WFS measurements were recorded. The controller used was alternatively a 6 parameter predictor and an optimized integrator. During each closed-loop period, 10 images were recorded by the imaging CCD camera to estimate S_r.

Using Zernike polynomial expansion, different parameters have been estimated from the SH WFS measurements to characterize the observing conditions: r_0, L_0, V and SNR. L_0 was stationary and of the order of 4 m, while r_0 was not stationary. r_0 values at 0.65 μm are presented in Fig. 7 as a function of time. r_0 varies between 5 and 15 cm, with a mean value of 9.3 cm. $V \approx 2$ m.s^{-1} and SNR ≈ 15.

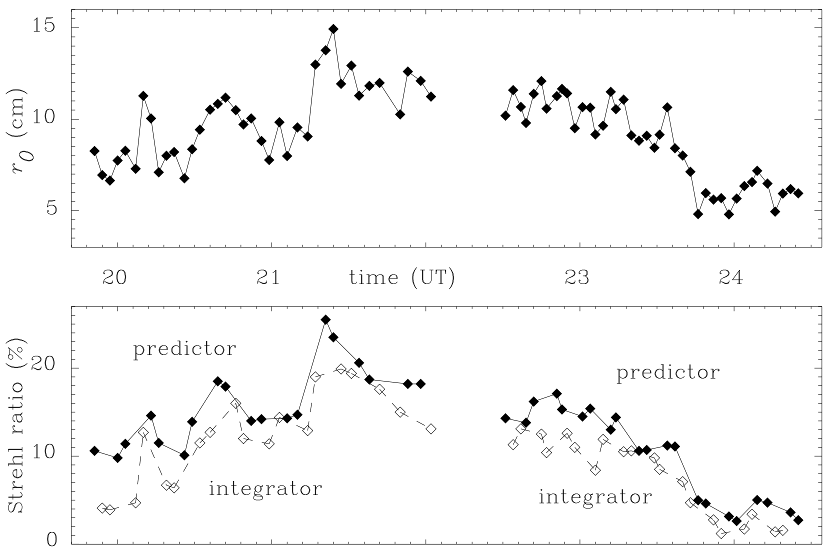

FIG. 7: *OHP experiment: r_0 and S_r computed at 0.65 μm when observing β Andromedae and ξ Cygni ($L_0 \approx 4$ m, $V \approx 2$ m/s). On the top graph, full and dotted curves correspond respectively to the predictive and the integral controllers.*

Fig. 7 shows the evolution of S_r as a function of time. From the comparison of the dotted curve (integrator) to the full curve (predictor), it comes out that the predictor is always more efficient than the integrator. The average relative gain is 30% for both β Andromedae and ξ Cygni. S_r is higher for higher r_0 since the turbulent variance is proportional to $(D/r_0)^{5/3}$. However, S_r does not seem to be affected by the value of f_s, which was 264 Hz for β Andromedae and 159 Hz for ξ Cygni. This is due to the very low value of V. The servo-loop bandwidth is not limiting the performance of the AO system because the cut-off frequency [12] of the power spectral density of the control modes is much lower than the system bandwidth. The bandwidth being proportional to the sampling frequency, there is no benefit to sample at 264 Hz rather than 159 Hz, except for SNR purposes. These results demonstrate the significant gain brought by the use of a modal predictive controller rather than a modal optimized integral controller, even in conditions where the AO system is not severely limited by its correction bandwidth.

To quantify the gain brought by the use of the predictor, it is reminded that S_r can be interpreted in terms of image SNR [19]. We find that a relative gain of 30% in S_r is equivalent to a relative gain of 3 in the corrected image SNR, at half the telescope aperture spatial cut-off frequency. The direct consequence of this is a gain of 10 in observing time by using a predictor rather than an integral controller for a given image SNR [19].

5.2 Filtering vibrations with a predictor

We report a second experiment which was carried out during the night from 09/28/97 to 09/29/97. Its aim was to test the capacity of the predictor to filter out a vibration at 75 Hz affecting tip-tilt modes, due to tracking errors of the telescope. This capacity to filter out a vibration is due to the fact that the transfer function of the predictor approaches the spectral signal-to-noise ratio of the signal when the residual phase variance is minimized. The binary star Deneb was observed at $f_s = 264$ Hz. While the deformable mirror was controlled by an integral controller of constant gain $K = 0.3$, the TTM was either controlled by an optimized integrator or a predictor.

Figure 8 shows the integral of a residual tip-tilt error measured by the SH WFS. The integral is defined as $I(f) = \int_{x=0}^{x=f} dsp(x)dx$ where $dsp(f)$ is the temporal power spectral density. The integrals have been normalized to the variance of the residual tip-tilt while the system was operating with the integrator. The jump observed for the integrator (dotted line) is due to the residual vibration which is not corrected. It disappears when using the predictor (full line). This clearly shows that the predictor has filtered out the vibration. The gain in terms of variance is $\approx 20\%$. Frequency transfer functions show that the expected attenuation is of the order of 20 dB around 75 Hz for the predictor, whereas the integrator cannot attenuate at all. It should be emphasized that the sampling frequency is 264 Hz, which means the vibration frequency is higher than the system bandwidth. The transfer functions of both controller are very similar, except at 75 Hz.

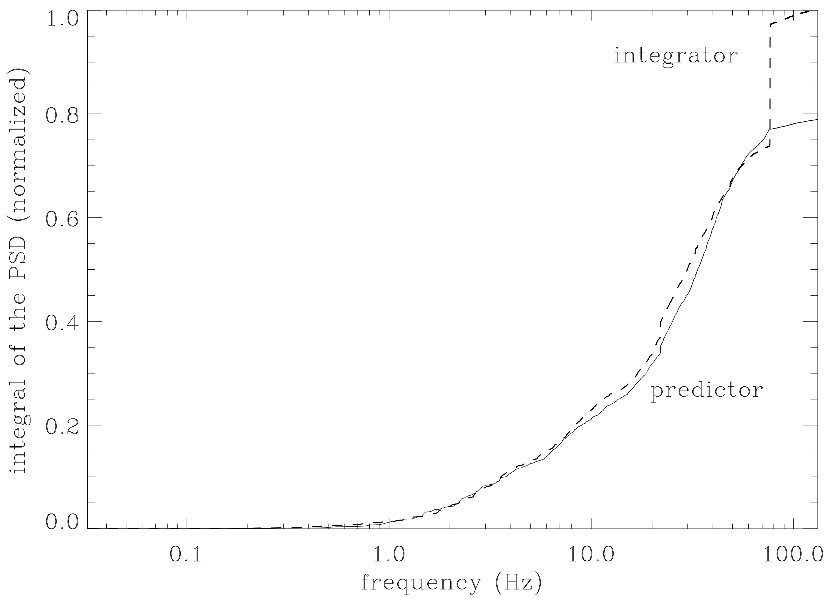

FIG. 8: *OHP experiment: integral of the power spectral density of one residual tip-tilt mode.*

6 Conclusion

This paper gives a general overview of the developments which led us from the theoretical approach to the experimental implementation of a modal linear predictor on an AO system operating in real conditions.

The modal linear predictor is a controller whose parameters minimize the residual mean square error of each control modes of the AO system. This minimization leads to a controller which best fits the spectral signal-to-noise ratio of the control modes. As expected, numerical simulations and laboratory experiments show that its efficiency depends on the ratio of the cut-off frequency of the control modes power spectral density to the sampling frequency. The higher the wind speed or the lower the sampling frequency, the more we gain by using a predictor rather than a classical optimized integrator. It is also more efficient in low measurement noise conditions, since a predictor cannot predict white noise.

For the first time, prediction has been tested on sky in real conditions to control an AO system. The predictor and the algorithm which is used to derive its parameters are robust and behave as expected. In the experimental conditions encountered at OHP, the gain brought by using the predictor instead of an optimized modal integrator can be as high as 10 in observing time. An other interesting characteristic of this predictor is its capacity to filter out vibrations due to tracking errors of the telescope or wind excitation of mechanical structures.

7 Acknowledgments

The authors wish to thank Laurent Rousset-Rouvière for the implementation of the predictor in the user-interface; François Charbonnier for helping us during laboratory experiments and the staff of Observatoire de Haute-Provence.

References

[1] B. Ellerbroek, C. V. Loan, N. Pitsianis, and R. Plemmons, "Optimizing closed loop adaptive optics performance using multiple control bandwidths," J. Opt. Soc. Am. A **11,** 2871 (1994).

[2] E. Gendron and P. Léna, "Astronomical adaptive optics I. Modal control optimization," Astron. Astrophys. **291,** 337 (1994).

[3] E. Gendron and P. Léna, "Astronomical adaptive optics II. Experimental results of an optimized modal control," Astron. Astrophys. **111,** 153 (1994).

[4] G. Aitken, D. Rossille, and D. McGaughey, "Predictability of fractional-Brownian-motion wavefront distortions and some implications for closed-loop adaptive optics control," In *Adaptive Optical System Technologies*, D. Bonaccini and R. Tyson, eds.,**3353,** 1060 (SPIE, Washington, 1998).

[5] M. Jorgenson and G. Aitken, "Prediction of atmospherically induced wave-front degradations," Opt. Lett. **17,** 466 (1992).

[6] D. Montera, B. Welsh, M. Roggemann, and D. Ruck, "Prediction of wave-front sensor slope measurements with artificial neural networks," Appl. Opt. **36,** 675 (1997).

[7] M. Lloyd-Hart and P. McGuire, "Spatio-temporal prediction for adaptive optics wavefront reconstructors," In *Proceedings of Topical Meeting on Adaptive Optics*, M. Cullum, ed.,**54,** 95 (ESO, Garching, Germany, 1995).

[8] D. Bonaccini, D. Gallieni, and R. Giampieretti, "Prediction of star wander path for adaptive optics," In *Proceedings of Topical Meeting on Adaptive Optics*, M. Cullum, ed.,**54,** 103 (ESO, Garching, Germany, 1995).

[9] C. Schwartz, G. Baum, and E. Ribak, "Turbulence-degraded wave fronts as fractal surfaces," J. Opt. Soc. Am. A **11,** 444 (1994).

[10] W. Wild, "Predictive optimal estimators for adaptive-optics systems," Opt. Lett. **21,** 1433 (1996).

[11] R. Paschall and D. Anderson, "Linear quadratic Gaussian control of a deformable mirror adaptive optics system with time-delayed measurements," Appl. Opt. **32,** 6347 (1993).

[12] C. Dessenne, P.-Y. Madec, and G. Rousset, "Optimization of a predictive controller for closed-loop adaptive optics," Appl. Opt. **37,** 4623 (1998).

[13] C. Dessenne, P.-Y. Madec, and G. Rousset, "Modal prediction for closed-loop adaptive optics," Opt. Lett. **22,** 1535 (1997).

[14] M. Demerlé, P. Madec, and G. Rousset, "Servo-loop analysis for adaptive optics," In *Adaptive Optics for Astronomy*, D. Alloin and J.-M. Mariotti, eds., NATO ASI Series C423 p. 73 (Kluwer Academic Publishers, Dordrecht, 1994).

[15] G. Franklin, J. Powell, and M. Workman, *Digital Control of Dynamic Systems* (Addison-Wesley, 1990).

[16] G. Rousset, P.-Y. Madec, and D. Rabaud, "Adaptive optics partial correction simulations for two telescope interferometry," In *High-Resolution Imaging by Interferometry*, J. Beckers and F. Merkle, eds., p. 1095 (ESO, Garching, Germany, 1991).

[17] M. Miller, P. Zieske, and D. Hanson, "Characterization of atmospheric turbulence," In *Imaging Through the Atmosphere*, **75,** 30 (SPIE, Washington, 1976).

[18] J.-M. Conan, G. Rousset, and P.-Y. Madec, "Wavefront temporal spectra in high resolution imaging through turbulence," J. Opt. Soc. of Am. A **12,** 1559 (1995).

[19] J.-M. Conan, P.-Y. Madec, and G. Rousset, "Image formation in adaptive optics partial correction," In *ICO-16 Satellite Conference on Active and Adaptive Optics*, F. Merkle, ed., p. 181 (ESO, Garching, Germany, 1993).